Chemically modified solid state nanopores for high throughput nanoparticle separation

2010 J. Phys.: Condens. Matter 22 454107

(http://iopscience.iop.org/0953-8984/22/45/454107)

IOP Publishing Journal of Physics: Condensed Matter

J. Phys.: Condens. Matter **22** (2010) 454107 (9pp) doi:10.1088/0953-8984/22/45/454107

Chemically modified solid state nanopores for high throughput nanoparticle separation

Anmiv S Prabhu[1], Talukder Zaki N Jubery[2], Kevin J Freedman[3], Rafael Mulero[3], Prashanta Dutta[2] and Min Jun Kim[1,3,4]

[1] School of Biomedical Engineering and Health Science, Drexel University, Philadelphia, PA 19104, USA
[2] School of Mechanical and Materials Engineering, Washington State University, Pullman, WA 99164, USA
[3] Department of Mechanical Engineering and Mechanics, Drexel University, Philadelphia, PA 19104, USA

E-mail: mkim@coe.drexel.edu

Received 31 March 2010, in final form 27 May 2010
Published 29 October 2010
Online at stacks.iop.org/JPhysCM/22/454107

Abstract

The separation of biomolecules and other nanoparticles is a vital step in several analytical and diagnostic techniques. Towards this end we present a solid state nanopore-based set-up as an efficient separation platform. The translocation of charged particles through a nanopore was first modeled mathematically using the multi-ion model and the surface charge density of the nanopore membrane was identified as a critical parameter that determines the selectivity of the membrane and the throughput of the separation process. Drawing from these simulations a single 150 nm pore was fabricated in a 50 nm thick free-standing silicon nitride membrane by focused-ion-beam milling and was chemically modified with (3-aminopropyl)triethoxysilane to change its surface charge density. This chemically modified membrane was then used to separate 22 and 58 nm polystyrene nanoparticles in solution. Once optimized, this approach can readily be scaled up to nanopore arrays which would function as a key component of next-generation nanosieving systems.

(Some figures in this article are in colour only in the electronic version)

1. Introduction

The ability to separate a specific population of molecules from a heterogeneous mixture is of vital importance to chemical and bio-analytical studies. For instance, being able to efficiently separate individual proteins from a mixture will greatly aid basic biochemical studies and applications thereof, such as proteomics and investigations of the biochemical pathways of various diseases like cancer. Currently standard techniques utilize an immobilized matrix, such as a gel or a chromatographic column, to separate individual fractions from a mixture. Such matrices contain randomly oriented pores with wide size distributions and provide little control on how they interact with analytes in order to achieve separation. This lack of engineering control is a major drawback of such techniques and greatly affects their efficiency [1]. However utilizing micro- and nanofabrication techniques it is possible to develop systems with finely controlled dimensions in the nanometer length scales. Within such systems the transport properties of nanoparticles can be closely controlled, thus making them ideally suited for efficient nanoparticle separation. As a result, over the past two decades several microfluidic and nanofluidic devices have emerged for the analysis and separation of nanometer-sized particles [1, 2]. Prominent among these are devices containing solid state nanopores fabricated in ultrathin ceramic membranes. Though such systems were first created to mimic biological pores in lipid bilayers for the detection and characterization of single biomolecules [3, 4], of late their potential for nanoparticle separation has also been recognized [5–8].

[4] Author to whom any correspondence should be addressed.

Within all micro- and nanofluidic systems, the large surface area to volume ratio makes surface-driven phenomena such as electrostatic forces especially dominant, resulting in unique transport properties that have received much attention in the recent past and have been the subject of many reviews [1, 2]. Thus, controlling the surface properties of such systems allows precise control over the transport of nanoparticles through them. Several such systems have been reported recently [6–8] among which, of special interest, is the work by Striemer *et al* who fabricated 10 nm thick nanoporous membranes and chemically modified them to achieve much better separation efficiency than conventional dialysis membranes [7]. Separation through such ultrathin membranes also tends to be faster owing to reduced transit times of the molecules being separated. Such devices have many potential biomedical applications such as in hemofiltration devices [9] and lipid apheresis devices.

The motivation behind the current work is to develop a generalized system that can eventually separate biomedically relevant molecules such as proteins and especially plasma lipoproteins. High levels of low density lipoproteins (LDL) in blood plasma can cause cardiac disorders such as atherosclerosis or even myocardial infarction. Current treatments include LDL apheresis [10], a procedure that utilizes a chemical affinity column to specifically filter these molecules from the blood plasma that also contains other lipoproteins. This procedure is both expensive and time-consuming and hence developing alternatives would be highly advantageous. The nanoparticles used as analytes in the current study closely resemble high density and low density lipoproteins in terms of their size and surface charge and since nanopore-based devices separate analytes based on these properties the ability to separate these nanoparticles should pave the way for low cost, ultra-fast LDL apheresis devices in the future.

In the present work we demonstrate the separation of polystyrene nanoparticles through a nanopore-based membrane system. However, rather than using an array of nanopores, we chose to study the separation of two differently sized nanoparticles through a membrane bearing only a single nanopore. We do this for two reasons. Firstly, utilizing the ionic current blockade technique, we can gather information about the size of the particles from the current signature they generate as they translocate the pore. From this it is possible to directly determine the efficiency of separation, thus eliminating the need for additional equipment such as a UV/vis spectrophotometer to detect the particles post-separation [11]. Secondly, such a system would be simpler to model and optimize for efficient separation and, once the optimal parameters are determined, they can be readily applied on a larger scale to nanosieves.

We first modeled the transport of a charged particle suspended in an electrolyte across an insulating membrane containing a single pore of comparable dimensions and studied the effect of the membrane surface charge on the particle velocity. Based on this model, a single nanopore was fabricated in an insulating silicon nitride membrane which was subsequently chemically modified with (3-aminopropyl)triethoxysilane to change its surface charge density. This chemically modified nanofluidic architecture was then used to separate 22 and 58 nm polystyrene nanoparticles.

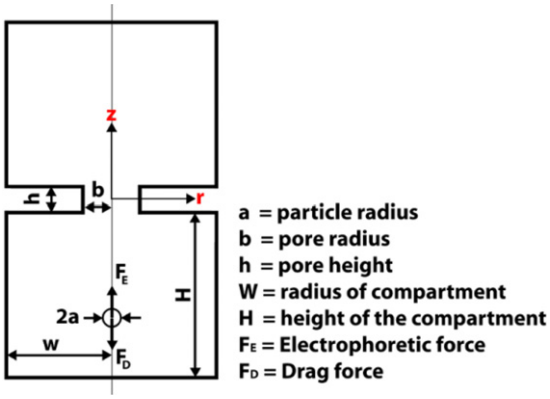

Figure 1. The experimental set-up was modeled as shown here. A cylindrical coordinate system with r and z as the radial and axial components was used. In addition to the dimensions noted here the surface charge density of the nanopore membrane and the translocating particle were set as σ_m and σ_p, respectively. Using this model we were able to analyze the effect of the surface charge density of the nanopore membrane on the particle's velocity as it crossed the nanopore as well as study fluctuations in the ionic current caused by the particle.

2. Mathematical model

In order to investigate the separation of nanoparticles by a nanopore membrane, the translocation kinetics of a nanoparticle in the vicinity of a nanopore were simulated. Two cylindrical compartments of radius W and height H, separated by an insulating membrane of height h, with a pore of diameter b containing a binary electrolyte were considered as shown in figure 1. One of the compartments contained a spherical particle of radius a and uniform surface charge density σ_p suspended in an electrolyte. The insulating membrane was assigned a surface charge density σ_m. A cylindrical coordinate system with radial coordinate r and axial coordinate z was defined with its origin at the center of the pore. Finally, a voltage difference was applied between $z = H$ and $-H$ that caused the particle to translocate across the pore.

The multi-ion model [12, 13] which uses continuum equations for the electrolyte and assumes a quasi-steady-state condition for the particle translocation was applied to the above system. The quasi-steady-state approximation is based on the short characteristic timescales of the electrostatics and the mass transport processes in the present study.

Based on the continuum approximation, the flow of an incompressible electrolyte in the compartment is governed by the Navier–Stokes (1) and continuity (2) equations:

$$\rho_f \left(\frac{\partial \vec{V}}{\partial t} + (\vec{V} \cdot \nabla)\vec{V} \right) = -\nabla P + \mu \nabla^2 \vec{V} + \rho_e \vec{E} \quad (1)$$

$$\nabla \cdot \vec{V} = 0 \quad (2)$$

where ρ_f, P and μ are the electrolyte density, pressure and viscosity, respectively. $\vec{E} = -\nabla\varphi$ is the electric field and ρ_e is the electric charge density, which is given by $\rho_e = \sum_1^N F z_i C_i$, where F, z_i and C_i are Faraday constant, valence and concentration of ith ionic species of the electrolyte, respectively.

Due to the low Reynolds number flow through the nanoscale device, the inertial term in equation (1) was neglected in this model. Atmospheric pressure was considered at the top and bottom boundaries ($z = \pm H$), a slip boundary condition was considered at $r = \pm W$ and a no-slip boundary condition was used at the membrane surface. At the nanoparticle surface the electrolyte velocity was set as the particle velocity.

The transport of ionic species of the electrolyte was described by the Nernst–Planck equation (3):

$$\frac{\partial C_i}{\partial t} + \nabla \cdot (-D_i \nabla C_i + \vec{V} C_i + z_i \omega_i \vec{E} C_i) = R_i \qquad (3)$$

where D_i, ω_i and R_i are the molecular diffusivity, mobility and chemical reaction rate of the ith ionic species in the flow field, respectively. In this model, equation (3) was simplified based on the quasi-steady-state approximation and the assumption that no chemical reaction occurs. Specified concentration was used at all boundaries of the compartments and zero flux was considered through the membrane walls and the nanoparticle surface.

Finally, the Poisson equation (4) with ε as the dielectric constant of the electrolyte was used to determine the potential distribution within our system:

$$\nabla \cdot (\varepsilon \nabla \varphi) = -\rho_e. \qquad (4)$$

Further, specified surface charge densities were set for the particle and membrane surfaces and a specified potential was assigned at all boundaries of the compartments. Since the simulated compartments are much smaller than those that would be used experimentally, the potential at the boundaries were approximated from the actual applied potential by solving the Laplace equation (5) for the experimental conditions:

$$\nabla \cdot (\kappa \nabla \phi) = 0 \qquad (5)$$

where ϕ and κ are the applied potential and conductivity of the electrolyte, respectively.

Next, equations (1)–(4) were solved simultaneously to determine the hydrodynamic drag force (6) and the electrostatic driving force (7) on the particle:

$$\vec{F}_D = \int\int_S [-PI + \mu(\nabla \vec{V} + (\nabla \vec{V})^T)] \cdot \vec{n}\, dS \qquad (6)$$

$$\vec{F}_E = \int\int_S \sigma_p \vec{E}\, dS \qquad (7)$$

where $\vec{F}_D = [F_{Dz}, F_{Dr}]$, $\vec{F}_E = [F_{Ez}, F_{Er}]$ and $\vec{n} = [n_r, n_z]$ is the unit normal vector on the particle surface and I is the unit tensor.

Assuming the particle is translocating along the centerline of the pore in the z direction, under a quasi-steady-state approximation, the particle velocity would satisfy equation (8):

$$F_{Dz} + F_{Ez} = 0. \qquad (8)$$

In order to numerically solve the above equations an initial value for particle velocity was assumed and equations (1)–(7) were used to compute the forces acting on the particle. Based on these values particle velocity was updated iteratively using the Newton–Raphson method until equation (8) was satisfied.

Finally, the ionic current through the nanopore J was calculated using equation (9), where A is the cross-sectional area of the nanopore:

$$J = \int\int_A \sum_{i=1}^{N} F z_i (-D_i \nabla C_i + \vec{V} C_i + z_i \omega_i \vec{E} C_i) \cdot d\vec{A}. \qquad (9)$$

In this model, the particle velocity is determined by balancing the electrostatic and viscous drag forces as shown in equation (8). The electrostatic driving force arises from the electrophoretic pull on the charged particle in an electric field while the viscous drag force arises from fluid flow due to the particle motion as well as the electro-osmotic flow (EOF) around the charged particle and the membrane surface. Since these forces are governed by the charge of the particle and the membrane, the dependence of the particle velocity on these parameters was investigated further for the case of a negatively charged particle and a negatively charged membrane, as were used in the experimental section of this study. In this case the EOF at the particle as well as the membrane surface creates a drag force that opposes the electrophoretic pull experienced by the particle and hence in order for the particle to translocate the pore the electrophoretic force must overcome the drag force created by the EOF. Since the surface charge density of membrane and particle both determine the forces acting on the particle, their effect on particle translocation was investigated individually.

First, the translocation of 22 nm and 58 nm particles with surface charge densities of -0.022 C m^{-2} and -0.011 C m^{-2}, respectively, suspended in 0.2 M KCl, across a 150 nm diameter pore was simulated for various membrane surface charge densities as shown in figure 2. A detailed description of the nanoparticles and the motivation behind using them in the current study is presented in section 3.3. We found that, at the surface charge density of bare silicon nitride [14], -0.02 C m^{-2}, the smaller 22 nm particle could cross the pore because its surface charge density was large enough for the electrophoretic force acting on it to overcome the drag force due to the EOF. On the other hand, the larger 58 nm particle had a lower surface charge density and experienced a lower electrophoretic force which was unable to overcome the component of the drag force arising from the EOF. As a result, solving equation (8) yielded a velocity vector that pointed away from the nanopore. Also, from our simulations we observe that the ionic current across the pore begins to drop from its baseline value when the translocating particle is ~150 nm from the center of the pore, well before it enters the nanopore, and only returns to its baseline value once the

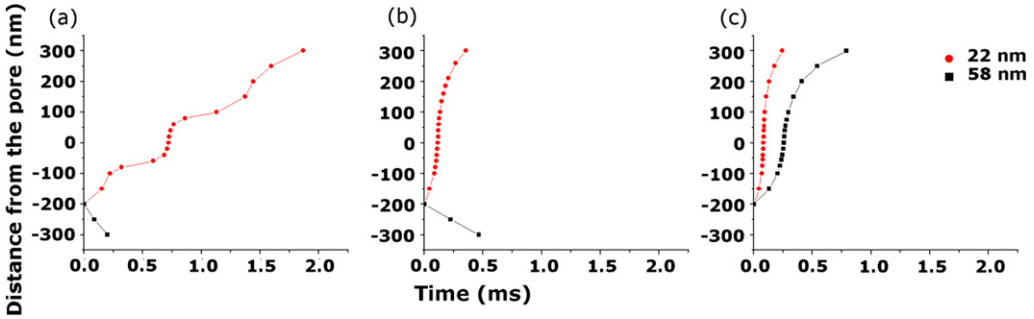

Figure 2. The surface charge density of the nanopore membrane greatly influences the velocity of the translocating particle in the vicinity of the pore and hence the selectivity of the membrane. The distance of the 22 and 58 nm particle from the center of the pore is plotted as a function of time for membranes with a surface charge density of (a) -0.02 C m^{-2}, (b) -0.015 C m^{-2} and (c) -0.008 C m^{-2}. For the surface charge density of bare silicon nitride, only the 22 nm particles translocate the pore but have a high residence time. At a lower surface charge density the membrane is still selective to 22 nm particles: however, they translocate much faster. At a surface charge density of -0.008 C m^{-2} both the particles are able to translocate the pore.

particle has crossed the pore and is ∼150 nm away. Since we rely on the blockage of ionic current to detect and characterize nanoparticles experimentally, the total translocation time of the particle is considered as the amount of time taken for the ionic current to drop from the baseline value and return back to it.

By this definition, the translocation time for the 22 nm particles in the current simulation was 1.7 ms. At a lower membrane surface charge density of -0.015 C m^{-2} the EOF at the membrane was reduced and while the membrane was still impermeable to the 58 nm particle the velocity of the 22 nm particle increased and its translocation time dropped to 0.17 ms. At an even lower surface charge density of -0.008 C m^{-2} the membrane was permeable to both the nanoparticles. From these simulations it was evident that by modulating the surface charge density of the nanopore membrane it was possible to alter its permeability to particles of different sizes and surface charge densities, thus allowing effective particle separation.

In order to determine the effect of particle surface charge density on the separation process, the translocation of 58 nm particles of different surface charge densities across a membrane with a surface charge density of -0.008 C m^{-2} was also simulated. The velocity of the particle at the beginning of the translocation event, that is, at a distance of 150 nm from the center of the pore, was determined for various surface charge densities as shown in figure 3. It was observed that, as the particle surface charge density became less negative, its velocity decreased until a surface charge density of -0.008 C m^{-2}. Below this value the particle could not translocate across the pore since the electrophoretic force on it was no longer able to overcome the EOF at the membrane surface.

Hence efficiency and throughput of the separation process were determined largely by the surface charge densities of the nanopore membrane as well as the translocating particles. For the particles used in the current study while bare silicon nitride membranes would allow particle separation, the throughput of the process would be low and in order to optimize the separation process for high throughput and maximum efficiency the surface charge density of our membranes needed to be around -0.015 C m^{-2}. The fabrication of our nanopores and the protocol used to modify their surface charge density are presented in section 3.

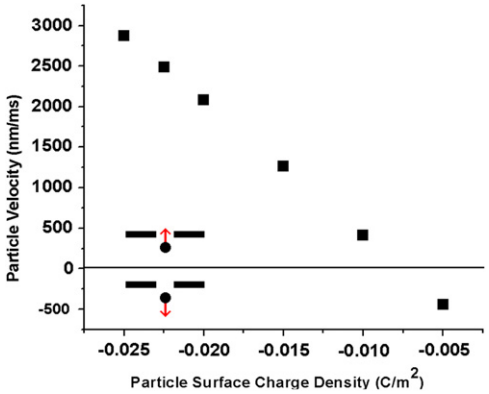

Figure 3. The electrophoretic and viscous drag forces acting on the translocating particle depend on its surface charge density as well. Depicted here is the velocity of a 58 nm particle at a distance of 150 nm from the center of the pore in a membrane with a surface charge density of -0.008 C m^{-2}, for various particle surface charge densities. As the surface charge density of the negatively charged particle decreases its velocity decreases due to a decrease in the electrophoretic force on it. At a surface charge density below -0.008 C m^{-2} the electrophoretic force on the particle cannot overcome the drag force created by the EOF at the membrane surface and hence the particle is unable to translocate the pore.

3. Material and methods

3.1. Nanopore fabrication

Over the last decade, several techniques to fabricate nanometer-sized pores in insulating membranes have been developed [15–18]. For our current work, nanopores were fabricated in ultrathin, free-standing silicon nitride membranes using focused-ion-beam milling. Our free-standing membranes were fabricated by first depositing a 50 nm thick layer of low-stress silicon nitride on a 340 μm thick silicon wafer using low pressure chemical vapor

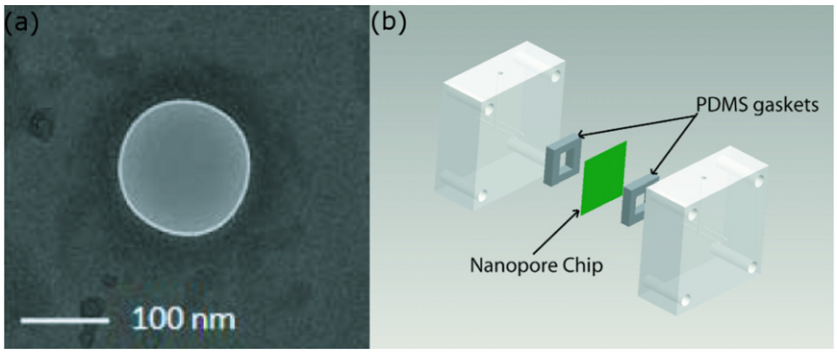

Figure 4. (a) A TEM image of a 150 nm solid state nanopore in a 50 nm thick low-stress silicon nitride membrane fabricated by FIB milling. By controlling the ion beam exposure time it is possible to reproducibly fabricate pores with a tolerance of ±10 nm. (b) A schematic of the flow cell used to house the nanopore chip. Electrolytic compartments are formed by cutting channels in the PDMS gaskets and these can be perfused via the inlet and outlet channels drilled in the polycarbonate cell.

deposition (LPCVD). This process was carried out at 825 °C using ammonia and dichlorosilane in a flow ratio of 1:5, resulting in a silicon-rich nitride film with tensile stress in the range of 50–150 MPa. Next, the silicon wafer was subject to photolithography, deep reactive ion etching (DRIE) and KOH wet etching to form a 50 × 50 μm^2, 50 nm thick free-standing silicon nitride membrane. Once the membranes were fabricated, a focused-ion beam (FEI Strata DB235) with an accelerating voltage of 30 keV and a 10 pA aperture was used to drill nanopores in them. Under these conditions, by adjusting the drill time it is possible to reproducibly fabricate pores ranging in size from 50 to >400 nm. For the current experiments we used a drill time of 1500 ms which resulted in a 150 ± 10 nm pore depicted in figure 4(a).

3.2. Modifying the nanopore surface

In solution, silicon nitride is known to acquire a negative surface charge density of -0.02 C m^{-2} [14] at neutral pH owing to the deprotonation of native silanol groups. According to our model this surface charge density is not optimal for high throughput separation of our nanoparticles. Because silanol groups have a pK_a value in the range of 4–4.3 [19], reducing the electrolyte pH below 4 would neutralize them and thus lower the surface charge density of the membrane. However, this could also destabilize our analyte molecules and was hence not a feasible option. Instead, we chose to modify our membranes by depositing 3-APTES which would react with the silanol groups and provide positively charged amine reactive groups to the membrane. The thickness and morphology of the deposited layer and number of accessible amine groups vary with the deposition technique used [20, 21]. Based on the work by Wang *et al* [21] we chose vapor deposition over solvent-based deposition.

Before the vapor deposition, the membranes were cleaned by boiling in piranha solution (H_2SO_4 and H_2O_2 in a ratio of 7:4 volume/volume) for 15 min and subsequently treated with oxygen plasma for 5 min (6.8 W, 101.6 kPa). The cleaned membranes were then placed in a vacuum chamber with 20 μl of 3-APTES (Sigma-Aldrich, Cat. #A3648) for 1 h and the deposited layer was annealed at 80 °C for 30 min.

3.3. Experimental set-up

The modified membranes were loaded into a custom-built polycarbonate flow cell with PDMS gaskets and Ag/AgCl electrodes. The electrodes were prepared by placing silver wires in bleach overnight and were placed in both half-cells. Channels were cut in the PDMS gaskets that held the electrolyte and the nanoparticle solutions, forming an electrolytic half-cell on either side of the insulating nanopore chip similar to the ones depicted in figure 1. The entire assembly was connected to the head stage of a patch clamp amplifier (Axopatch 200B, Molecular Devices Inc.) and housed in a Faraday cage. Figure 4(b) shows an exploded schematic of our assembled flow cell.

While the current work is on the separation of polystyrene nanoparticles, in the future we also aim to separate other biologically relevant molecules, like proteins, especially the high density and low density lipoproteins found in blood plasma. Hence in this study negatively charged 22 and 58 nm sulfate-functionalized polystyrene beads (Molecular Probes Cat. #S37202 and Cat. #S37200) were used as analytes. These beads have a surface charge density of 1.1 μC cm^{-2} and 2.2 μC cm^{-2}, respectively, and hence closely resemble the low density and high density plasma lipoproteins in terms of the ratio of their size and surface charge [22]. Since differences in size and surface charge are the main criterion for nanopore-based separation, we hypothesize that, if our set-up is able to separate these polystyrene nanoparticles, lipoprotein separation should also be possible. Dilutions of these beads were prepared in 0.2 M KCl and 1% Triton X-100 (Fisher Scientific Cat. #AC21586-2500) was used to prevent aggregation. The beads were serially diluted from the commercially available stock solution in 0.2 M KCl and used at a final concentration of 10^5 particles ml^{-1}. At each step of the dilution process, the bead solution was sonicated to ensure homogenization and prevent aggregation.

The 0.2 M KCl solution was prepared in deionized water and used as the electrolyte in the flow cell. While it would have been ideal to use a lower salt concentration which was closer to that found in blood plasma, this would have lowered the conductance of the cell and hence decreased the signal-to-noise ratio in our experiments. On the other hand, a higher

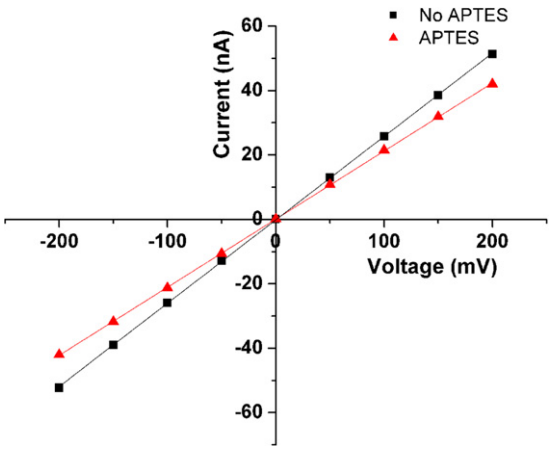

Figure 5. IV curves were plotted for the nanopore before and after chemical modification by recording the average current at regular voltage steps for a 10 s period. While the IV relation remains linear in the tested voltage range, the conductance of the pore was found to decrease from 0.256 to 0.211 μS post-chemical modification.

salt concentration would greatly reduce the Debye length of the charged polystyrene beads, thus causing them to aggregate and possibly clog the nanopore. As a result, we chose to carry out all our characterization and separation experiments at 0.2 M KCl.

4. Results and discussion

4.1. Characterizing the nanopore

Within our flow cell the only possible route for ions to travel between the electrolytic compartments is through the nanopore. Thus at a fixed electrolyte salt concentration the shape, dimensions and surface charge of the nanopore govern the conductance and current voltage dependence of the cell. In order to determine the current voltage dependence in our set-up and the effect of the 3-APTES deposition, we measured the conductance of the cell before and after the chemical modification process. The applied voltage across the pore was held constant for 10 s each from -200 to 200 mV in 50 mV steps while the current across the pore was recorded. The average current value for each voltage was used to plot the I–V curve in figure 5. Since the I–V relation was linear in this range the slope of this curve gives the conductance of the cell according to Ohm's law.

We found that, though 3-APTES deposition did not change the shape of the I–V curve, the conductance of the pore decreased from 0.256 to 0.211 μS. Considering only geometric effects this difference in conductance can be used to determine the approximate thickness of the 3-APTES layer deposited on the inside of the nanopore. With an initial pore diameter of $d = 150$ nm a 3-APTES thickness of $t \approx 7$ nm was obtained from equation (10), where S_1 and S_2 are the initial and final conductances, respectively. A more thorough analysis would also include the surface charge density of the deposited 3-APTES layer: however, for the current work this value was not experimentally derived. For our simulations a value of -0.015 C m^{-2} was assumed [21]:

$$\frac{d-2t}{d} = \sqrt{\frac{S_2}{S_1}}. \tag{10}$$

4.2. Data acquisition and analysis

To study nanoparticle separation, a mixture of 22 and 58 nm polystyrene beads was introduced into the anodic half-cell at a concentration of 10^5 particles ml^{-1}. When a voltage bias of 350 mV was applied across the nanopore and a 10 kHz low pass Bessel filter was applied, we observed the transient drops in current shown in figure 6(a). These drops were not observed in the absence of the nanoparticles and were hence attributed to the translocation of the polystyrene beads across the nanopore. From our simulations, the expected current drop caused by the 22 nm particles was ~600 pA. Hence, a threshold of 500 pA was set and only current blockades greater than this value were considered in the subsequent analysis. In this manner we identified roughly 1600 translocation events in a span of 15 min, after which the pore was irreversibly clogged.

The Coulter counter principle states that the current blockade caused by a particle as it translocates a pore depends on its size [23]. The estimated current drop for the 22 nm particles according to our simulations was ~600 pA and, though in our simulations the 58 nm beads did not translocate the pore, considering only geometric effects, the estimated current drop for these beads was ~4 nA. In order to analyze the experimental data statistically, each event was characterized in terms of the maximum current drop and duration of the blockade. Distributions of these parameters shown in figure 7(c) reveal a single mode at 680 pA and 0.09 ms which are close to the values expected for the 22 nm beads. Also from figure 7(a) it is evident that less than 1% of the observed events had a current drop around 4 nA. Thus, it was concluded that the majority of the current blockades were caused by the 22 nm beads going through the pore. This membrane selectivity can be explained by the fact the 58 nm beads have a lower surface charge density as compared to the 22 nm beads and hence experience a lower electrostatic pull which is unable to overcome the viscous drag force caused by the EOF developed by the surface of the charged membrane. As a result, solving equations (1)–(7) for a 58 nm bead yields a velocity vector that points away from the nanopore. Thus in the simulations, for our applied voltage and membrane surface charge density the 58 nm beads cannot translocate across the nanopore. Experimentally, however, the few observed events with a current blockade of ~4 nA can be accounted for by considering variability in the specified surface charge density of the 58 nm beads and an error in the assumed value of the membrane surface charge density.

The current signature caused by the 22 nm particle as it translocates the pore was also simulated, shown in red in figure 8(a), and found to be in good agreement with experimentally obtained events. Figure 8(b) depicts a typical large current blockade event that is presumed to have been caused by a 58 nm bead. The symmetric reverse Gaussian shape of the current blockades is a result of the symmetry in the

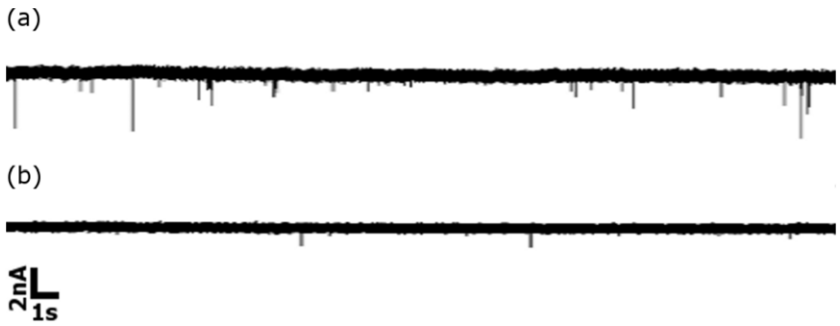

Figure 6. (a) Drops in the current across the chemically modified nanopore were observed when the nanoparticle mixture was introduced into the anodic half-cell. The frequency of these events is much higher than that observed with an unmodified pore shown in (b).

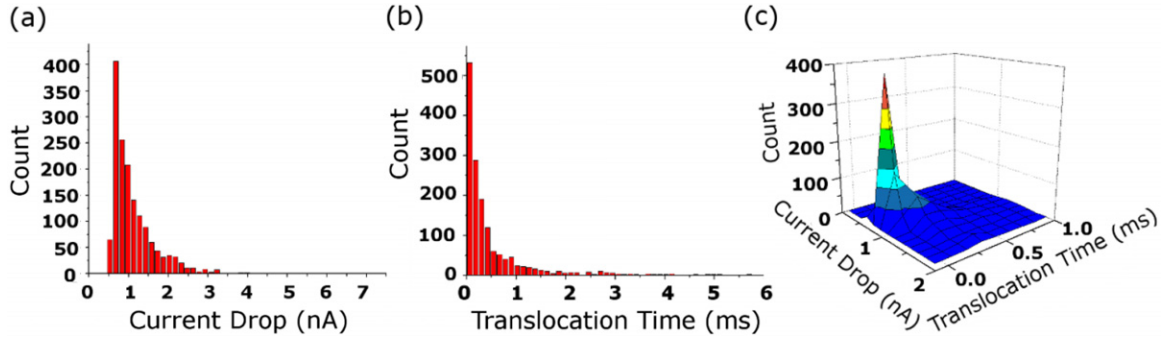

Figure 7. All the observed translocation events were analyzed in terms of the amplitude and time duration of the current blockade. (a) and (b) depict histograms of these parameters individually and their combined density distribution is plotted in (c). From these plots it is evident that the most populous events have a current drop of ∼600 pA and a translocation time of ∼0.25 ms, which are in good agreement with the simulated values for the 22 nm beads. Moreover, very few events with a current drop of 4 nA, which is expected from the 58 nm particles, were recorded.

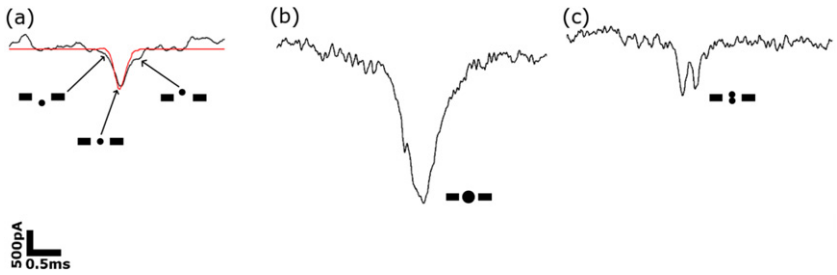

Figure 8. Shown here are the typical current signatures observed. The red line in (a) is a simulated current drop caused by a 22 nm particle and is in good agreement with the experimentally recorded current drops. The symmetric inverted Gaussian profile of the current signature is a result of the spherical shape of the translocating particle. The current signature in (b) is believed to have been caused by a single 58 nm particle translocating the pore while that in (c) is by two 22 nm particles translocating sequentially. The insets in (a) are schematics of the particle position with respect to the pore and the resulting level of current blockage, for a particle translocating from the lower compartment to the upper compartment as shown in figure 1. The insets in (b) and (c) are the presumed particle size and conformation that could have caused the corresponding current signatures. The schematics are not drawn to scale.

shape of the spherical polystyrene beads as shown in the insets. In addition to these two typical current signatures we also observed more complex signatures which are believed to have been caused by multiple beads simultaneously going through the pore in various conformations. For example, the current blockade depicted in figure 8(c) is believed to have been caused by two 22 nm beads translocating the pore sequentially. Such events coupled with the electrical noise in our set-up are believed to be responsible for the higher kurtosis of the current drop and translocation time distributions in figures 7(a) and (b), respectively. Surprisingly, no instances of multiple 58 nm beads or 22 and 58 nm beads crossing the pore simultaneously were observed.

Another advantage of coating our membranes with 3-APTES is the increase in the number of observed translocation events. When a similar experiment was performed with an uncoated pore, shown in figure 6(b), only a few hundred events were recorded in a similar time frame before the

pore was clogged. This observation can be explained by considering that the change in surface charge density caused by 3-APTES increases the velocity of the translocating particle, thus decreasing its net residence time within the pore as shown in figure 2(b). This not only increases the number of translocation events per unit time but also decreases the chances of a particle interacting with and getting lodged inside the pore. Similar observations of an increase in translocation events have also been reported by various groups using both organic α-hemolysin pores [24, 25] and inorganic solid state nanopores [7].

5. Conclusion

In this work we have demonstrated the potential application of solid state nanopores as a nanoparticle separation platform. From a mathematical description of the translocation process, the surface charge density of the nanopore membrane was recognized as an important parameter in determining its selectivity. Simulations revealed that, though the surface charge density of our silicon nitride membrane made it selectively permeable to only one of our two analytes, it was not optimal for high throughput separation. As a result, our membranes were modified by depositing 3-APTES so as to lower their surface charge density and achieve more translocation events. The experimentally obtained current blockages for the translocating particles were in good agreement with those simulated, and from their distribution it was evident that the majority of these blockages were caused by the 22 nm particles as they translocated the pore. At the same time the translocation of the 58 nm particles was almost completely prevented since the reduced electrostatic attraction, due to lower surface charge density, could not overcome the viscous drag force contributing from the EOF created at the charged membrane surface. An important motivation behind the current work was to eventually develop better platforms to separate plasma lipoproteins owing to many health problems caused by excess low density lipoproteins and the many drawbacks of the current LDL apheresis systems. Since the nanoparticles chosen as analytes in the current work closely resemble HDL and LDL in terms of the ratios of their size and surface charge we believe that our set-up holds great promise in this regard.

In the future we aim to control the membrane surface charge density more accurately by calibrating the vapor deposition process and experimenting with different silanes to control the morphology of the deposited layer as well [21]. This process, once optimized, can then be applied to nanosieves to develop generalized high throughput separation platforms. An alternative approach being considered is to use an external gating potential similar to Nam *et al* [8]. Regardless of the technique used, such experiments are an important step towards developing next-generation devices for nanoparticle and biomolecule separation and analysis. Given the recent growth in the field of nanoparticles and their emergence in the commercially available products, such devices will be important in the future to monitor and regulate the use of nanoparticles and understand their impact on the environment.

Acknowledgments

This work was supported by the Human Frontier Science Program Young Investigator Award RGY0075/2009-C. The authors are also grateful to Dr Zhorro Nikolov at the Centralized Research Facilities, Drexel University for his valuable insights.

References

[1] Fu J, Mao P and Han J 2008 Artificial molecular sieves and filters: a new paradigm for biomolecule separation *Trends Biotechnol.* **26** 311–20
[2] Bohn P W 2009 Nanoscale control and manipulation of molecular transport in chemical analysis *Annu. Rev. Anal. Chem.* **2** 279–96
[3] Kasianowicz J J, Brandin E, Branton D and Deamer D W 1996 Characterization of individual polynucleotide molecules using a membrane channel *Proc. Natl Acad. Sci. USA* **93** 13770–3
[4] Movileanu L, Howorka S, Braha O and Bayley H 2000 Detecting protein analytes that modulate transmembrane movement of a polymer chain within a single protein pore *Nat. Biotechnol.* **18** 1091–5
[5] Vidal J, Gracheva M and Leburton J-P 2007 Electrically tunable solid-state silicon nanopore ion filter *Nanosc. Res. Lett.* **2** 61–8
[6] Cees J M v R *et al* 1998 Nanosieves with microsystem technology for microfiltration applications *Nanotechnology* **9** 343
[7] Striemer C C, Gaborski T R, McGrath J L and Fauchet P M 2007 Charge- and size-based separation of macromolecules using ultrathin silicon membranes *Nature* **445** 749–53
[8] Nam S-W, Rooks M J, Kim K-B and Rossnagel S M 2009 Ionic field effect transistors with sub-10 nm multiple nanopores *Nano Lett.* **9** 2044–8
[9] Conlisk A, Datta S, Fissell W and Roy S 2009 Biomolecular transport through hemofiltration membranes *Ann. Biomed. Eng.* **37** 722–36
[10] Thompson G R 2003 LDL apheresis *Atherosclerosis* **167** 1–13
[11] Surugau N and Urban P L 2009 Electrophoretic methods for separation of nanoparticles *J. Sep. Sci.* **32** 1889–906
[12] Qian S, Wang A and Afonien J K 2006 Electrophoretic motion of a spherical particle in a converging–diverging nanotube *J. Colloid Interface Sci.* **303** 579–92
[13] Chein R and Dutta P 2009 Effect of charged membrane on the particle motion through a nanopore *Colloids Surf.* A **341** 1–12
[14] Sonnefeld J 1996 Determination of surface charge density parameters of silicon nitride *Colloids Surf.* A **108** 27–31
[15] Kim M J, McNally B, Murata K and Meller A 2007 Characteristics of solid-state nanometre pores fabricated using a transmission electron microscope *Nanotechnology* **18** 205302
[16] Kim M J, Wanunu M, Bell D C and Meller A 2006 Rapid fabrication of uniformly sized nanopores and nanopore arrays for parallel DNA analysis *Adv. Mater.* **18** 3149–53
[17] Storm A J, Chen J H, Ling X S, Zandbergen H W and Dekker C 2003 Fabrication of solid-state nanopores with single-nanometre precision *Nat. Mater.* **2** 537–40
[18] Li J, Stein D, McMullan C, Branton D, Aziz M J and Golovchenko J A 2001 Ion-beam sculpting at nanometre length scales *Nature* **412** 166–9
[19] Chaiyasut C, Takatsu Y, Kitagawa S and Tsuda T 2001 Estimation of the dissociation constants for functional

groups on modified and unmodified silica gel supports from the relationship between electroosmotic flow velocity and pH *Electrophoresis* **22** 1267–72

[20] Rathor N and Panda S 2009 Aminosilane densities on nanotextured silicon *Mater. Sci. Eng.* C **29** 2340–5

[21] Wang W and Vaughn M W 2008 Morphology and amine accessibility of (3-aminopropyl) triethoxysilane films on glass surfaces *Scanning* **30** 65–77

[22] Sparks D and Phillips M 1992 Quantitative measurement of lipoprotein surface charge by agarose gel electrophoresis *J. Lipid Res.* **33** 123–30

[23] DeBlois R and Bean C 1970 Counting and sizing of submicron particles by the resistive pulse technique *Rev. Sci. Instrum.* **41** 909

[24] Wolfe A J, Mohammad M M, Cheley S, Bayley H and Movileanu L 2007 Catalyzing the translocation of polypeptides through attractive interactions *J. Am. Chem. Soc.* **129** 14034–41

[25] Maglia G, Restrepo M R, Mikhailova E and Bayley H 2008 Enhanced translocation of single DNA molecules through α-hemolysin nanopores by manipulation of internal charge *Proc. Natl Acad. Sci.* **105** 19720–5